Radboud Repository

Radboud University Nijmegen

PDF hosted at the Radboud Repository of the Radboud University Nijmegen

The following full text is a preprint version which may differ from the publisher's version.

For additional information about this publication click this link.
http://hdl.handle.net/2066/199274

Please be advised that this information was generated on 2019-06-02 and may be subject to change.

DISCOVERY OF ^{14}NH$_3$ (2,2) MASER EMISSION IN SGR B2-MAIN

E. A. C. MILLS
Physics Department, Brandeis University, 415 South Street, Waltham, MA 02453, USA

A. GINSBURG
National Radio Astronomy Observatory[2] 1003 Lopezville Rd Socorro, NM 87801, USA

A. R. CLEMENTS
Department of Chemistry, University of Virginia, Charlottesville, VA, 22904, USA

P. SCHILKE
I. Physikalisches Institut, Universität zu Köln, Zülpicher Str. 77, D-50937 Köln, Germany

Á. SÁNCHEZ-MONGE
I. Physikalisches Institut, Universität zu Köln, Zülpicher Str. 77, D-50937 Köln, Germany

K. M. MENTEN
Max-Planck-Institut für Radioastronomie, Auf dem Hügel 69, 53121 Bonn, Germany

N. BUTTERFIELD
Green Bank Observatory, 155 Observatory Rd, PO Box 2, Green Bank, WV 24944, USA

C. GODDI
Department of Astrophysics/IMAPP, Radboud University, PO Box 9010, 6500 GL Nijmegen, The Netherlands

A. SCHMIEDEKE
Max-Planck Institute for Extraterrestrial Physics, Giessenbachstrasse 1, D-85748 Garching, Germany

C. G. DE PREE
Department of Physics & Astronomy, Agnes Scott College, 141 E. College Ave., Decatur, GA 30030, USA
Draft version November 30, 2018

ABSTRACT

We report the discovery of the first ^{14}NH$_3$ (2,2) maser, seen in the Sgr B2 Main star forming region near the center of the Milky Way, using data from the Very Large Array radio telescope. The maser is seen in both lower resolution (3″ or ∼0.1 pc) data from 2012 and higher resolution (0″.1 or ∼1000 AU) data from 2018. In the higher resolution data NH$_3$ (2,2) maser emission is detected toward 5 independent spots. The maser spots are not spatially or kinematically coincident with any other masers in this region, or with the peaks of the radio continuum emission from the numerous ultracompact and hypercompact H II regions in this area. While the (2,2) maser spots are spatially unresolved in our highest resolution observations, they have unusually broad linewidths of several kilometers per second, which suggests that each of these spots consists of multiple masers tracing unresolved velocity structure. No other NH$_3$ lines observed in Sgr B2 Main are seen to be masers, which continues to challenge existing models of NH$_3$ maser emission.

1. INTRODUCTION

elisabeth.ac.mills@gmail.com
[1] A. Ginsburg is a Jansky Fellow of the National Radio Astronomy Observatory.
[2] The National Radio Astronomy Observatory is a facility of the National Science Foundation operated under cooperative agreement by Associated Universities, Inc.

Ammonia masers are relatively rare, and have been seen in only a handful of sources, mainly high-mass star forming regions. Despite this rarity, many different ^{14}NH$_3$ (J, K) inversion transitions, both nonmetastable $(J \neq K)$ and metastable $(J = K)$, have been observed to be masers (e.g., Wilson & Schilke 1993). Maser action has even been reported to occur in a transition of the rare isotopologue ^{15}NH$_3$ (Mauersberger et al. 1986; Johnston et al. 1989; Gaume et al. 1991; Schilke et al.

1991).

$^{14}NH_3$ masers arising from nonmetastable energy levels are more frequently seen than metastable masers. This is likely due to the smaller population of these levels, which quickly decay unless excited by extreme densities or intense radiation fields and are thus easier to invert (Wilson & Schilke 1993). The most common of these appear to be in the ortho-NH_3 ($K = 3n$) transitions (9,6) and (6,3) (Madden et al. 1986; Pratap et al. 1991; Wilson & Schilke 1993). However, few surveys for nonmetastable $^{14}NH_3$ masers are reported in the literature (Madden et al. 1986 report surveying 17 regions for maser emission but only finding masers in 4 of these), and ultimately these masers have only been reported toward 5 regions: W51, W49, DR21, NGC 7538, and NGC 6334. Additional masing nonmetastable transitions, including para-NH_3 transitions, have been observed in W51 (Mauersberger et al. 1987; Wilson & Henkel 1988; Wilson et al. 1990; Henkel et al. 2013), NGC 7538 (Hoffman & Kim 2011; Hoffman & Joyce 2014), and NGC 6334 (Walsh et al. 2007).

Of the metastable $^{14}NH_3$ masers, the most commonly observed masing transition is the ortho (3,3) line, which has been definitively seen toward DR21(OH), W51-North, and G5.89-0.39 (Mangum & Wootten 1994; Zhang & Ho 1995; Hunter et al. 2008), and which has been suggested to also be a maser in a variety of other sources, including NGC 6334, the southern part of Sgr B2, and the nucleus of the starburst galaxy NGC 253 (Kraemer & Jackson 1995; Martin-Pintado et al. 1999; Ott et al. 2005). Other ortho lines – (6,6), (9,9), and (12,12)– have also been reported to exhibit maser action in NGC 6334 (Walsh et al. 2007) and W51 (Henkel et al. 2013; Goddi et al. 2015). Para-NH_3 masers are rarer, however masers have been reported in the (1,1) line toward the DR21 H II region (Gaume et al. 1996), in the (5,5) line toward G9.62+0.19 (Hofner et al. 1994) and in the (7,7) line toward W51 North(Goddi et al. 2015).

We report the discovery of a new, strong para-$^{14}NH_3$ maser in the metastable (2,2) transition toward the Galactic center star forming region Sgr B2 Main, hereafter Sgr B2 (M). Sgr B2 is the most massive molecular cloud in the central 500 parsecs of the Galaxy, accounting for 10% of the mass in this region (Scoville et al. 1975). This cloud hosts the most intense ongoing star formation in the Galactic center, much of which is concentrated in two sites of clustered star formation: Sgr B2 (M) and Sgr B2 North or (N). Sgr B2 (M) is suggested to be older than Sgr B2 (N), as it is less chemically rich (Corby et al. 2015; Sánchez-Monge et al. 2017) and appears more fragmented (Qin et al. 2011; Sánchez-Monge et al. 2017; Ginsburg et al. 2018). In addition to containing a fragmented, massive hot core (Vogel et al. 1987; Qin et al. 2011; Sánchez-Monge et al. 2017), it contains dozens of ultracompact and hypercompact H II regions (De Pree et al. 1998). Sgr B2 (M) also contains at least one molecular outflow traced by H_2O masers, $^{14}NH_3$ emission and absorption, and millimeter H_2CO lines (Vogel et al. 1987; McGrath et al. 2004; Qin et al. 2008). In this paper, we present new, high-resolution centimeter-wave observations of $^{14}NH_3$ toward this region, and discuss the detected (2,2) maser emission both in the context of other star formation indicators detected in this specific region, and in the context of NH_3 masers in general.

2. DATA

2.1. Low-resolution observations

Observations of $^{14}NH_3$ toward Sgr B2 (M) were made using the Karl G. Jansky Very Large Array (VLA), a facility of the National Radio Astronomy Observatory[1] in January 2012 in DnC configuration using the K band receivers (project 11B-210, PI: E.A.C. Mills). For the $^{14}NH_3$ (2,2) line at 23.7226333 GHz, the synthesized beam size was $2''.83 \times 2''.56$, which corresponds to a spatial resolution of 0.1 pc at the adopted distance to Sgr B2 of 8 kpc (Reid et al. 2009; Gravity Collaboration et al. 2018). The velocity resolution of the (2,2) line observations was 1.58 km s^{-1}. In addition to the (2,2) line, the (1,1) through (7,7) and (9,9) metastable $^{14}NH_3$ lines were also observed, along with the (10,9) nonmetastable line. The observations toward the Sgr B2 cloud were part of a larger survey of Galactic center clouds; additional description of these observations, including details on the data calibration and imaging, is given in Mills et al. (2015).

2.2. High-resolution observations

Observations of $^{14}NH_3$ toward Sgr B2 (M) were also made using the A configuration of the VLA in March-April 2018 (project 18A-229, PI: A. Ginsburg). These observations had a spatial resolution of $0''.17 \times 0''.08$ (1360×640 AU) and a velocity resolution of 0.79 km s^{-1} for the (2,2) line. Other observed lines of $^{14}NH_3$ included (1,1), (2,2), (4,4), (5,5), (7,7), (2,1), (3,2), (5,3), and (5,4), however the (3,2) line was not observed in all sources as it was on the edge of a sub-band which limited the frequency coverage.

The data were pipeline processed using the VLA pipeline after removing the automated RFI flagging step. We then performed three iterations of phase-only self-calibration using the brightest $^{14}NH_3$ (2,2) maser peak.

2.3. Absolute positional reference frame

We define the absolute positional reference frame for these observations using a high-resolution ($0''.2$), 3 mm ALMA continuum map (Project code 2016.1.00550.S, PI: A. Ginsburg) which should have good absolute positional accuracy as it is tied to a larger mosaic of the region (Ginsburg et al. 2018). We use the task 'register_translation' from the python package scikit-image (van der Walt et al. 2014) to perform cross correlations between the ALMA image and our A-configuration continuum image, and shift our A-configuration images by $0''.05$ in Right Ascension and $0''.48$ in Declination. The uncertainty in the alignment from the cross correlation is $\pm 0''.03$. This large offset is due to an error in the VLA calibrator catalog for the position of source J1744-3116, which is used as a phase calibrator for the A-configuration data (L. Sjouwerman, private comm.).
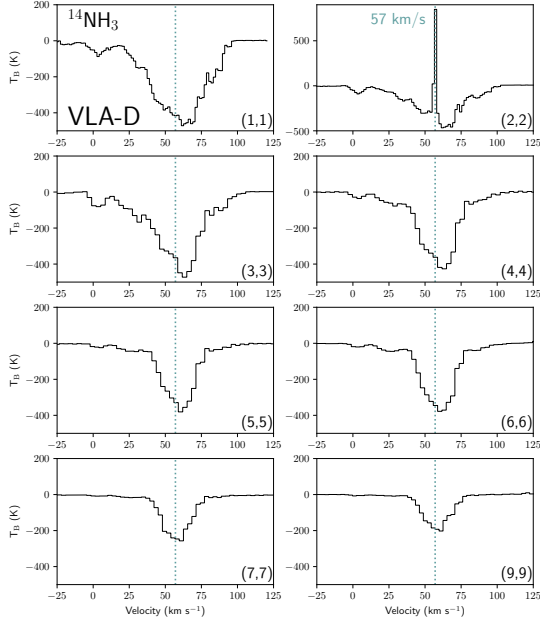
3. RESULTS

Fig. 1.— Spectra of $^{14}NH_3$ metastable transitions from VLA D-configuration observations. All transitions are seen in absorption against the 'F' complex of H II regions in Sgr B2 (M) except the (2,2) line, where maser emission is also seen at a velocity of 57 km s^{-1}. This velocity is indicated by a vertical dotted line in each panel.

Of the 13 observed transitions of $^{14}NH_3$ (10 of which were observed in A configuration), we detect maser emission in only the (2,2) line[1]. The A-configuration observations of $^{14}NH_3$ (5,4) also overlap with the $^{15}NH_3$ (2,2) line, which we can confirm does not show similar maser emission. In Figure 1 we show spectra from the D-configuration observations in which we see a single, narrow (the line is unresolved for a channel width of 1.5 km s^{-1}) maser component at 57 km s^{-1}, in the midst of broad absorption that is seen in all of the observed $^{14}NH_3$ lines. In the A configuration, this maser breaks up into 5 independent spots spread out over 2″ at velocities from 57 to 69 km s^{-1}, with measured velocity widths of 1.6-3.9 km s^{-1}. We show spectra of all the $^{14}NH_3$ lines toward the brightest maser spot in Figure 2, and profiles of the (2,2) line toward each of the 5 detected maser spots in Figure 3. The (2,2) maser appears to be a persistent feature over a large time baseline, as it is not only seen in our 2012 and 2018 observations, but can be seen in Figure 6 of Vogel et al. (1987), where there is a negative

[1] We investigate other possible line identifications for this maser, and find that there only three species that have been detected toward Sgr B2 (M) that have transitions lying within ~10 km s^{-1} of the (2,2) line: HCOOCH$_3$ (and its isotopologue H^{13}COOCH$_3$ which has not been detected but is likely present), ^{17}OH and CH$_3$OCH$_3$. However, none of these are a plausible candidate for this maser, as these species have either never been observed to be masers in the ISM (^{17}OH and CH$_3$OCH$_3$) or have only been observed to be weak masers with widths similar to those of thermally excited lines (Faure et al. 2014), which is inconsistent with the narrower profiles seen in our observations.
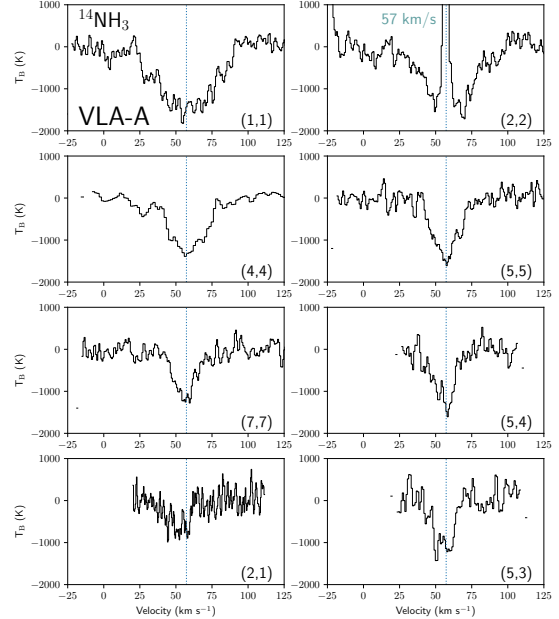

Fig. 2.— Spectra of $^{14}NH_3$ metastable and nonmetastable transitions from VLA A-configuration observations toward the position of Maser M1, the strongest (2,2) maser spot. All transitions are seen in absorption against the 'F' complex of H II regions in Sgr B2 (M) except the (2,2) line, where the maser emission is seen at a central velocity of ~57 km s^{-1} (vertical dotted line). The y-axis of all of the plots has been scaled to the same range to emphasize the absorption present in all transitions; the peak of the (2,2) maser emission is 9×10^4 K.

optical depth (i.e., emission) at a velocity of ~ 60 km s^{-1}.

The positions of the $^{14}NH_3$ masers are shown in Figure 4. The brightest maser is M1, which has a peak intensity of 0.5 Jy, or a brightness temperature of $T_B > 9 \times 10^4$ K.[2] M2 is only slightly offset from M1, and its spectrum contains an additional emission contribution from the sidelobes of M1; it may peak nearer to a velocity of 59 km s^{-1} with $T_B > 7000$ K. M3 is offset by ~ 1″ from M1 and has $T_B > 3900$ K. M4 and M5 are much weaker, having limits on T_B of only $> 700 K$. While this could be considered consistent with thermal emission, as temperatures > 1000 K have been measured toward Sgr B2 (M) (Wilson et al. 2006), no correspondingly bright emission is seen in the other NH$_3$ lines, indicating that these sources are also nonthermal. Maser spots M1-M4 are on the edge of continuum sources, and the maser emission toward these regions is superimposed on a broad absorption feature. However, M5 is not near to any known continuum source, and shows a weak thermal emission rather than absorption profile in the other NH$_3$ lines. In Table 1 we list the properties of each detected maser spot, including its position, central velocity, velocity width, and peak brightness temperature.

Based on the correspondence between the absorption

[2] All listed brightness temperatures are lower limits, as the maser spots are spatially unresolved.

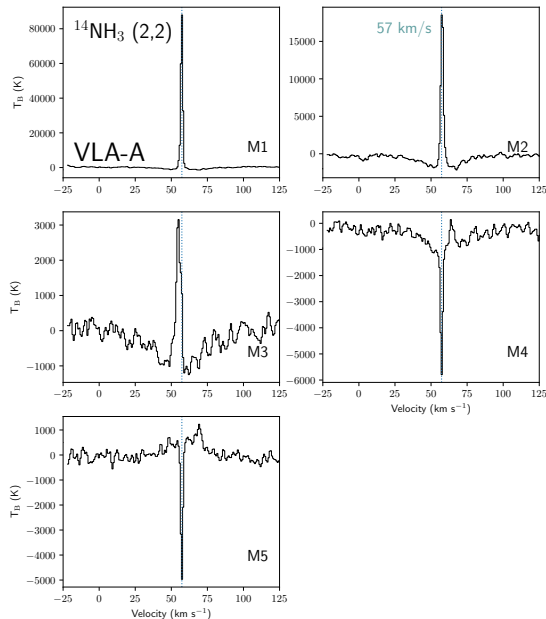| Source	Right Ascension	Declination	v_{cen} (km s^{-1})	v_{fwhm} (km s^{-1})	Peak T$_{MB}$ (K)
M1	$17^h47^m20^s.167\pm0.001$	$-28°23'4''.36\pm0.01$	57.22 ± 0.01	1.64 ± 0.02	90900 ± 1000
M2	$17^h47^m20^s.177\pm0.001$	$-28°23'4''.52\pm0.02$	57.68 ± 0.04	2.13 ± 0.10	21100 ± 800
M3	$17^h47^m20^s.113\pm0.002$	$-28°23'4''.11\pm0.04$	54.99 ± 0.20	3.89 ± 0.47	3900 ± 400
M4	$17^h47^m20^s.200\pm0.001$	$-28°23'4''.92\pm0.02$	64.05 ± 0.51	2.15 ± 1.19	700 ± 300
M5	$17^h47^m20^s.101\pm0.001$	$-28°23'5''.52\pm0.02$	69.21 ± 0.46	3.43 ± 1.09	700 ± 200

FIG. 3.— Spectra of the ^{14}NH$_3$ (2,2) line toward each of the maser spots seen in the A-configuration data. Maser spots M1-4 are superimposed on absorption against nearby H II regions, while M5 lies on top of a broad, thermal emission profile. The central velocity of M1, the brightest maser source, is shown as a vertical dotted line at 57 km s^{-1} in each panel. The narrow absorption at this velocity seen in the spectra of M4 and M5 is an artifact from the sidelobes of M1.
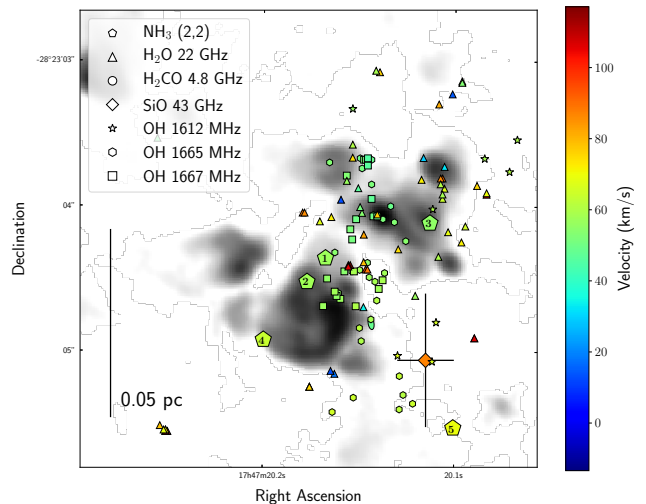

FIG. 4.— Position of the ^{14}NH$_3$ (2,2) masers detected toward Sgr B2 (M), overlaid on a 3 mm ALMA continuum map (Project 2016.1.00550.S, PI: A. Ginsburg). Also shown are the positions of published maser detections from H$_2$O (McGrath et al. 2004), OH (Gaume & Claussen 1990), SiO (Morita et al. 1992), and H$_2$CO (Mehringer et al. 1994). Only the OH masers brighter than 1 Jy are shown, due to the large number detected in this region. The positions of all masers except SiO are determined relative to the continuum emission, and should have positional uncertainty $< 0''.5$, smaller than the plotted points. The H$_2$CO maser emitting region is partially resolved and plotted as an ellipse.

and emission seen in the A-configuration observations, we believe it is most likely that the main hyperfine component[1] of the (2,2) line is masing (while this is assumed for most observed ^{14}NH$_3$ masers, the only observed 1,1 maser occurs in an outer hyperfine satellite component; Gaume et al. 1996). The maser velocity is also consistent with the velocity of relatively narrow metastable line emission seen in the D-configuration observations $4''$ to the west. However, the maser velocity is not consistent with the velocity of ^{14}NH$_3$ metastable and non-metastable line emission observed $3''$ to the south, which appears to be closer to 70 km s^{-1}.

Comparing the maser positions to the radio continuum in Figure 4, we do not see a clear correspondence between these masers and radio continuum: only four of the five masers overlap with continuum emission, and these tend to be located on the edge of the H II regions in Sgr B2 (M). Interestingly, M1 is located within $0''.2$ of an increase in continuum emission from source 'F3c' detected in De Pree et al. (2014). We also compare the position of the (2,2) masers to a number of other masers, both rare and common, that are also seen in Sgr B2 (M). This includes 1612, 1665, and 1667 MHz OH masers (Gaume & Claussen 1990), 22 GHz H$_2$O masers (McGrath et al. 2004), a 4.8 GHz H$_2$CO maser (Mehringer et al. 1994), and a 43 GHz $J = 1 - 0, v = 1$ SiO maser (Morita et al. 1992). We have used published figures of the masers and the simultaneously observed continuum emission to align the maser positions with our continuum maps. We adjust the positions of the H$_2$O masers by $+0''.16$ in Right Ascension and $+0''.54$ in Declination to match our reference frame. We also adjust the position of the OH masers by $+0''.84$ in Declination and the H$_2$CO maser by $+0''.42$ in Declination. No corresponding continuum map for the 43 GHz SiO maser is published in (Morita et al. 1992), so we adopt their published position and estimates of the absolute positional uncertainty. The position of these

---

[1] The inner and outer hyperfine satellites in the (2,2) line are offset from the main hyperfine line component by ±16.6 and ±25.8 km s^{-1}, respectively.

other masers relative to the (2,2) masers is shown in Figure 4. None of the other masers observed in Sgr B2 (M) appear to overlap with the (2,2) maser in both position and velocity, though there is a weak ($< 2Jy$) OH 1665 MHz maser within $0''.1$ of M1 and offset by ~ 5 km s^{-1}.

4. DISCUSSION

4.1. Interpreting the (2,2) maser in Sgr B2 (M)

This is the first ^{14}NH$_3$ (2,2) maser seen in any source. It is a relatively strong maser, with brightness temperatures constrained to be $> 10^4$ K by the A-configuration observations. This is among the brightest ^{14}NH$_3$ masers that have been reported, which typically have limits on their brightness temperatures of $> 10^2 - 10^5$ K (Madden et al. 1986; Wilson et al. 1991; Mangum & Wootten 1994; Hofner et al. 1994; Zhang & Ho 1995; Gaume et al. 1996; Hunter et al. 2008; Walsh et al. 2007; Hoffman & Kim 2011; Hoffman & Joyce 2014; Goddi et al. 2015), with only a single VLBI measurement of the ^{14}NH$_3$ (9,6) maser having a brightness temperature $> 10^{13}$ K(Pratap et al. 1991).

The most unique characteristic of the observed (2,2) masers is their linewidth. In the A-configuration observations, line profiles of individual maser spots are well resolved, having widths of up to 4 km s^{-1}. Narrow ($<$1km s^{-1}) or unresolved widths are typical of most other observed NH$_3$ masers. As individual masers show nonthermal linewidths, we must assume multiple masers are present, and that the extreme or unique physical conditions that lead to these masers are relatively common in this region. Given that both the (2,2) masers and the nearby SiO maser show relatively broad linewidths over a compact region, an intriguing possibility is that these masers could arise in or near rotating protostellar disks (e.g., as in the SiO masers around Orion's source I; Goddi et al. 2009; Matthews et al. 2010)

Given limits on the observed maser spot sizes of $\lesssim$1000 AU, the observed (2,2) maser line widths could be consistent with Keplerian rotation in the disk of a low- or intermediate-mass protostar. A line width of 2-4 km s^{-1} for a disk with a radius of 400 AU would be consistent with rotation around a central mass of 0.5-2 M$_\odot$. In the future, one might be able to test whether the ^{14}NH$_3$ masers arise from such organized or compact circumstellar structures by making VLBI observations of these masers. However, such low mass protostellar sources would be difficult to detect in millimeter continuum emission as imaging near the bright sources in this region is significantly limited by an achievable dynamic range of $\sim$5000 with ALMA (Ginsburg et al. 2018).

4.2. The Excitation of the (2,2) Maser

Our observations suggest that maser emission is possible in essentially any metastable transition of ^{14}NH$_3$: of the inversion transitions up to $J = 9$, only the (4,4) and (8,8) lines have not yet been observed to show maser action, though a weak ^{15}NH$_3$ (4,4) maser has been reported (Schilke et al. 1991). However at present, no universally successful mechanism has been proposed for NH$_3$ masers. Suggested models for NH$_3$ maser excitation involve three possible mechanisms (1) radiative excitation from 10 μm continuum emission, (2) collisional excitation, and (3) radiative excitation from a chance line overlap.

Current models of nonmetastable maser emission favor mechanism (1): excitation through the 10 μm vibrational transitions pumped by infrared emission (Brown & Cragg 1991). However, these theories tend to predict that multiple, adjacent transitions of NH$_3$ should mase simultaneously (Wilson & Schilke 1993). While masers have been seen in adjacent nonmetastable transitions (Henkel et al. 2013; Hoffman & Joyce 2014), and metastable transitions of ortho-NH$_3$ (e.g., 6,6 and 9,9 masers; Goddi et al. 2015), no sources have been observed to show maser emission in multiple para-NH$_3$ transitions. The only published model of a metastable NH$_3$ involves the second mechanism, pumping the ortho (3,3) transition via collisions with H$_2$ (Flower et al. 1990; Mangum & Wootten 1994). However, this model does not predict masers in metastable transitions of para NH$_3$ (Schilke et al. 1991), and cannot explain observations of simultaneous maser emission in the ortho- (4,3) and (3,3) lines of ^{15}NH$_3$ (Schilke et al. 1991). Mechanism (3), line overlap, is not currently favored to explain any of the observed NH$_3$ masers (e.g., as discussed in Goddi et al. 2015). Indeed, the detection of maser emission in the (2,2) line makes this more unlikely as a general mechanism to explain the metastable para-NH$_3$ masers, as separate instances of line overlap would be needed to pump each of the (1,1), (2,2), (5,5), and (7,7) lines.

As none of the existing three simple models provide a satisfactory explanation for these masers, we suggest that the excitation of the metastable para-NH$_3$ masers is likely complicated, and may require a confluence of geometry, velocity structure and possibly both collisional and radiative excitation (rotational and rovibrational transitions of NH$_3$ occur at a range of infrared wavelengths from 9 μm to 400 μm, and the vibrational transitions in particular may be influenced by the shape of the overlapping 9.7 μm silicate absorption feature, as noted by Barentine & Lacy 2012). Devising and validating such a complex model will likely require the availability of collisional coefficients for states above $J = 6$, which is the limit of currently published data (e.g., Bouhafs et al. 2017).

4.3. The (2,2) Maser as a Probe of Star Forming Regions

As ^{14}NH$_3$ is a common probe of gas in star forming regions, particularly the (1,1) and (2,2) lines, it is somewhat surprising that masers in this line have not previously been seen. Lu et al. (2014) surveyed 62 high-mass star forming regions in the ^{14}NH$_3$ (1,1) and (2,2) lines with subparsec spatial resolution using the VLA's DnC configuration and did not report any (2,2) maser emission. With an 800 K brightness temperature for this maser in our DnC-configuration observations, similar masers in other star forming regions should have been readily apparent. It appears likely then that, like other metastable ^{14}NH$_3$ masers, this maser is quite rare, which would limit its general usefulness as a star formation probe.

The (2,2) maser is the first NH$_3$ maser confirmed to exist in Sgr B2. This increases the number of star forming regions known to host either metastable or non-metastable NH$_3$ masers from 7 to 8. We suggest that

more massive star forming regions should be carefully surveyed for NH_3 masers in a wide variety of non-metastable and metastable transitions to better understand their overall incidence and association with various stages and structures of star formation, and to provide improved constraints for models of NH_3 maser excitation.

5. SUMMARY

We report the discovery of the first $^{14}NH_3$ (2,2) maser, which is detected in the Sgr B2 Main star forming region. Below, we summarize our main findings.

- At the high resolution of our VLA A-configuration observations ($0''.1$ or ~ 1000 AU) the (2,2) maser breaks into 5 independent spots with T_B from 700-

9×10^4 K. These $^{14}NH_3$ masers are not spatially or kinematically coincident with any other masers in this region, or with the peaks of the observed radio continuum emission.

- The $^{14}NH_3$ (2,2) masers are spatially unresolved in the A-configuration observations but have unusually broad linewidths of 1.5-4 km s^{-1}, which could trace the kinematics of circumstellar gas.

- The (2,2) maser is the only $^{14}NH_3$ maser seen in this region and the fourth metastable transition of para-$^{14}NH_3$ observed to be a maser, which increases the inconsistencies between the observed NH_3 masers and the existing models for this emission.

REFERENCES

Barentine, J. C., & Lacy, J. H. 2012, ApJ, 757, 111
Bouhafs, N., Rist, C., Daniel, F., et al. 2017, MNRAS, 470, 2204
Brown, R. D., & Cragg, D. M. 1991, ApJ, 378, 445
Corby, J. F., Jones, P. A., Cunningham, M. R., et al. 2015, MNRAS, 452, 3969
De Pree, C. G., Goss, W. M., & Gaume, R. A. 1998, ApJ, 500, 847
De Pree, C. G., Peters, T., Mac Low, M.-M., et al. 2014, ApJ, 781, L36
Faure, A., Remijan, A. J., Szalewicz, K., & Wiesenfeld, L. 2014, ApJ, 783, 72
Flower, D. R., Offer, A., & Schilke, P. 1990, MNRAS, 244, 4P
Gaume, R. A., & Claussen, M. J. 1990, ApJ, 351, 538
Gaume, R. A., Johnston, K. J., Nguyen, H. A., et al. 1991, ApJ, 376, 608
Gaume, R. A., Wilson, T. L., & Johnston, K. J. 1996, ApJ, 457, L47
Ginsburg, A., Bally, J., Barnes, A., et al. 2018, ApJ, 853, 171
Goddi, C., Greenhill, L. J., Chandler, C. J., et al. 2009, ApJ, 698, 1165
Goddi, C., Henkel, C., Zhang, Q., Zapata, L., & Wilson, T. L. 2015, A&A, 573, A109
Gravity Collaboration, Abuter, R., Amorim, A., et al. 2018, A&A, 615, L15
Henkel, C., Wilson, T. L., Asiri, H., & Mauersberger, R. 2013, A&A, 549, A90
Hoffman, I. M., & Joyce, S. A. 2014, ApJ, 782, 83
Hoffman, I. M., & Kim, S. S. 2011, ApJ, 739, L15
Hofner, P., Kurtz, S., Churchwell, E., Walmsley, C. M., & Cesaroni, R. 1994, ApJ, 429, L85
Hunter, T. R., Brogan, C. L., Indebetouw, R., & Cyganowski, C. J. 2008, ApJ, 680, 1271
Johnston, K. J., Stolovy, S. R., Wilson, T. L., Henkel, C., & Mauersberger, R. 1989, ApJ, 343, L41
Kraemer, K. E., & Jackson, J. M. 1995, ApJ, 439, L9
Lu, X., Zhang, Q., Liu, H. B., Wang, J., & Gu, Q. 2014, ApJ, 790, 84
Madden, S. C., Irvine, W. M., Matthews, H. E., Brown, R. D., & Godfrey, P. D. 1986, ApJ, 300, L79
Mangum, J. G., & Wootten, A. 1994, ApJ, 428, L33

Martin-Pintado, J., Gaume, R. A., Rodríguez-Fernández, N., de Vicente, P., & Wilson, T. L. 1999, ApJ, 519, 667
Matthews, L. D., Greenhill, L. J., Goddi, C., et al. 2010, ApJ, 708, 80
Mauersberger, R., Henkel, C., & Wilson, T. L. 1987, A&A, 173, 352
Mauersberger, R., Wilson, T. L., & Henkel, C. 1986, A&A, 160, L13
McGrath, E. J., Goss, W. M., & De Pree, C. G. 2004, ApJS, 155, 577
Mehringer, D. M., Goss, W. M., & Palmer, P. 1994, ApJ, 434, 237
Mills, E. A. C., Butterfield, N., Ludovici, D. A., et al. 2015, ApJ, 805, 72
Morita, K.-I., Hasegawa, T., Ukita, N., Okumura, S. K., & Ishiguro, M. 1992, PASJ, 44, 373
Ott, J., Weiss, A., Henkel, C., & Walter, F. 2005, ApJ, 629, 767
Pratap, P., Menten, K. M., Reid, M. J., Moran, J. M., & Walmsley, C. M. 1991, ApJ, 373, L13
Qin, S.-L., Schilke, P., Rolffs, R., et al. 2011, A&A, 530, L9
Qin, S.-L., Zhao, J.-H., Moran, J. M., et al. 2008, ApJ, 677, 353
Reid, M. J., Menten, K. M., Zheng, X. W., Brunthaler, A., & Xu, Y. 2009, ApJ, 705, 1548
Sánchez-Monge, Á., Schilke, P., Schmiedeke, A., et al. 2017, A&A, 604, A6
Schilke, P., Walmsley, C. M., & Mauersberger, R. 1991, A&A, 247, 516
Scoville, N. Z., Solomon, P. M., & Penzias, A. A. 1975, ApJ, 201, 352
van der Walt, S., Schonberger, J. L., Nunez-Iglesias, J., et al. 2014, PeerJ, 2, e453
Vogel, S. N., Genzel, R., & Palmer, P. 1987, ApJ, 316, 243
Walsh, A. J., Longmore, S. N., Thorwirth, S., Urquhart, J. S., & Purcell, C. R. 2007, MNRAS, 382, L35
Wilson, T. L., Gaume, R., & Johnston, K. J. 1991, A&A, 251, L7
Wilson, T. L., & Henkel, C. 1988, A&A, 206, L26
Wilson, T. L., Henkel, C., & Hüttemeister, S. 2006, A&A, 460, 533
Wilson, T. L., Henkel, C., & Johnston, K. J. 1990, A&A, 229, L1
Wilson, T. L., & Schilke, P. 1993, In: Astrophysical masers; Proceedings of the Conference, 412, 123
Zhang, Q., & Ho, P. T. P. 1995, ApJ, 450, L63